Optical and Quantum Electronics (2006) 38:217–230
DOI 10.1007/s11082-006-0005-x

A new differential method applied to the study of arbitrary cross section microstructured optical fibers

PHILIPPE BOYER*, GILLES RENVERSEZ, EVGENY POPOV AND MICHEL NEVIÈRE
Institut Fresnel, Case 161, Unité Mixte de Recherche Associée au Centre National de la Recherche Scientifique (UMR 6133), Université Paul Cézanne Aix-Marseille III et Université de Provence, Faculté des Sciences et Techniques de St. Jérôme, Avenue Escadrille Normandie Niémen, 13397 Marseille Cedex 20, France
*(*author for correspondence: E-mail: philippe.boyer@fresnel.fr)*

Received 29 September 2005; accepted 1 February 2006

Abstract. The present work adapts a recent grating theory called "Fast Fourier factorization" to cylindrical coordinates in order to study microstructured optical fibers (MOFs). Compared with the classical differential method, this new differential method takes into account the truncation of Fourier series and the discontinuities of the fields across the diffracting surface with the help of new factorization rules. The main advantage of this method is that the directrix of the diffracting cylindrical surface is arbitrary and permits anisotropic and inhomogeneous media although its numerical application needs longer computation time, compared with other well-known numerical methods. The S-propagation algorithm is used to avoid numerical contaminations. The numerical results are validated and compared with the well-established Multipole method in the case of a MOF with six circular cylinders. Further, a new cross-sectional profile (with sectorial inclusions) that the Multipole method cannot consider is studied.

Key words: Differential methods, Fast Fourier Factorization method, Microstrucutred optical fibers, Multipole method, Arbitrary cross section

1. Introduction

The properties of the microstructured optical fibers (MOFs) have been well studied with the numerical method called the Multipole Method (Kuhlmey *et al*. 2002; White *et al.* 2002; Zolla *et al*. 2005). However, this method has limitations: the inclusions must be disjoined circular cylinders and the matrix must be homogeneous and isotropic. To this aim, we are interested in a new differential method called Fast Fourier Factorization (FFF) adapted in cylindrical coordinates (Nevière *et al*. 2003; Boyer *et al*. 2004), in order to consider more complex MOF shapes. However, we begin with simpler cases when the media are homogeneous and isotropic. In the first part, the main key points of the theory are treated and introduced in matrix form. In fact the basic idea of the FFF is to use new factorization rules (Li 1996a) in Fourier space to rewrite the constitutive relation between the **D** vector and the electric field. Then, a new formulation of Maxwell

equations in the truncated Fourier space is deduced. Finally, the present boundary-value problem is changed into an initial value problem using a shooting method. The use of the S-propagation algorithm (Li 1996b) avoids numerical contaminations and leads to the S-matrix method. The effective index of the mode thus becomes a zero of the determinant of the S-matrix. The eigenvectors associated to null eigenvalues of the S-matrix attributed to these effective indices describe the modal fields of the studied MOF. In the second part, our first numerical results are shown: They include a MOF with six circular cylinders which permits us to validate the FFF method by comparison with the Multipole Method (MM) results. We also test the convergence with respect to the development order (truncation of the series) in order to illustrate the improvement of the FFF method compared to the classical differential one (Vincent *et al.* 1972). Finally, new results concerning a six sectorial cylinder MOF are presented.

2. The Fast Fourier Factorization method in cylindrical coordinates

2.1. PRESENTATION OF THE PROBLEM

We study a device described by a cylindrical surface S. Thus we are placed into both a Cartesian coordinate system Oxyz with $(\mathbf{e}_x, \mathbf{e}_y, \mathbf{e}_z)$ unit vectors and in cylindrical coordinates r, θ, z with $(\mathbf{e}_r, \mathbf{e}_\theta, \mathbf{e}_z)$ as unit vectors. The arbitrary directrix of the surface (S) located in the cross-sectional plane (Oxy), is defined by the equation $f(r, \theta) = 0$ or $r = g(\theta)$ (f and g are known functions) and either may contain the origin as shown in Fig. 1 or may not (see Fig. 2). Generatrices are straight lines parallel to the z-axis. Both regions separated by the surface S are filled with linear, homogeneous, isotropic dielectric and non-magnetic media. The interior medium, noted as (int), has a complex permittivity ε_{int} and the exterior one, noted as (ext), has a real permittivity ε_{ext}.

The Fast Fourier Factorization method is a differential method which uses a development of any opto-geometrical quantity as Fourier series with respect to the angular variable θ, since the cylindrical coordinate system naturally implies a 2π-periodicity with respect to θ. Moreover, we suppose that the total electromagnetic field has a harmonic $\exp(-i\omega t)$ time dependence and an $\exp(i\beta z)$ z-dependence, where β is the propagation constant. Therefore we can express any opto-geometrical quantity as

$$u(r, \theta, z, t) = \exp[i(\beta z - \omega t)] \sum_{n=-N}^{+N} u_n(r) \exp(in\theta) \tag{1}$$

in which $\omega = 2\pi/\lambda_0\sqrt{\mu_0\varepsilon_0}$. The truncation to the Nth order of this development is justified by the numerical application of the present method. In

addition, the space is divided in three regions by the inscribed circular cylinder of the surface S with directrix $C_{\min}$ and the circumscribed circular cylinder of the surface S with the directrix $C_{\max}$ (see Fig. 1 and 2). The purpose of the Fast Fourier Factorization is then to find the best formulation of the Fourier developments of the fields taking into account the discontinuities of these fields through the surface S and the truncation of the series, in the region included between both circular cylinders named "modulated area".

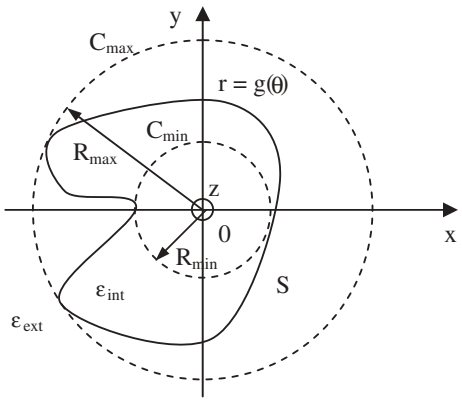

Fig. 1. Cylindrical object including the origin and notations.

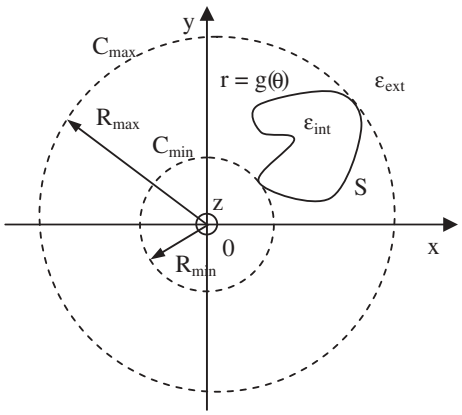

Fig. 2. Cylindrical object centered outside the origin and notations.

2.2. NEW FORMULATION OF THE MAXWELL EQUATIONS IN THE TRUNCATED FOURIER SPACE

At first, the linear constitutive relation between the **D** vector and the electric field is rewritten in the truncated Fourier space and in the modulated area with the help of new factorization rules. Then we inject this new relation into Maxwell equations in order to derive a set of first-order differential equations suitable for numerical computations.

In the modulated area, the constitutive relation in which the permittivity can be described by a 2π-periodic with respect to θ function $\varepsilon(r,\theta)$, is written as

$$\mathbf{D} = \varepsilon(r,\theta)\mathbf{E} \tag{2}$$

The Fourier development of the **D** vector is then expressed according to the product of the Fourier developments of the $\varepsilon(r,\theta)$ function and the electric field. While the classical differential method (Vincent *et al.* 1972) uses Laurent's rule (initially set for infinite Fourier developments, resulting in Fourier series) to write this constitutive relation in the truncated Fourier space, the Fast Fourier factorization method applies new factorization rules established by L. Li (Li 1966a) taking into account the truncation and the discontinuities of the $\varepsilon(r,\theta)$ function and the electric field. In the linear formulation of the present electromagnetic theory, we use a matrix notation in the truncated Fourier space: the column vector containing the Fourier components $\tilde{f}_n (n \in [-N,+N])$ of a function $\tilde{f}(x)$ is noted as $[\tilde{f}]$. The factorization rules apply to Fourier components $\tilde{h}_n$ of the product $\tilde{h}(x)$ of two periodic, piecewise-smooth, bounded functions $\tilde{f}(x)$ and $\tilde{g}(x)$. The first rule states that Laurent's rule is only valid in the truncated Fourier space when $\tilde{f}(x)$ and $\tilde{g}(x)$ are not simultaneously discontinuous at the same value of x:

$$\left[\tilde{f}\tilde{g}\right] = \left[\!\left[\tilde{f}\right]\!\right][\tilde{g}] \tag{3}$$

where $[\![\tilde{f}]\!]$ is the Toeplitz matrix of the function f defined by $([\![\tilde{f}]\!])_{n,m} = \tilde{f}_{n-m}$. The second rule states that a product of two piecewise-smooth, bounded, periodic functions that have only pairwise-complementary jump discontinuities (i.e. that have a continuous product) cannot be factorized by Laurent's rule, but can be factorized by the inverse rule:

$$\left[\tilde{f}\tilde{g}\right] = \left[\!\left[\frac{1}{\tilde{f}}\right]\!\right]^{-1}[\tilde{g}] \tag{4}$$

And finally, when a product of two piecewise-smooth, bounded, periodic functions have discontinuities at the same value of x with non-complemen-

tary jump discontinuities, such a product can be correctly factorized neither by Laurent's rule, nor by the inverse rule. In the relation (2), the electric field is split into its normal component $\mathbf{E_N}$ and its tangential component $\mathbf{E_T}$. The first factorization rule is applied to the tangential component $\mathbf{D_T}$ of $\mathbf{D}$ since $\mathbf{E_T}$ is continuous across (S). The second factorization rule is applied to the normal component $\mathbf{D_N}$ of $\mathbf{D}$ since $\mathbf{E_N}$ is discontinuous across (S) with $\mathbf{D_N}$ continuous across (S). The relation (2) rewrites $[\mathbf{D}] = [\![\varepsilon]\!][\mathbf{E_T}] + [\![\frac{1}{\varepsilon}]\!]^{-1}[\mathbf{E_N}]$. Expressing the $\mathbf{E_T}$ and the $\mathbf{E_N}$ components through the electric field and the normal vector $\mathbf{N}$ to the surface (S) ones, we finally obtain:

$$[\mathbf{D}] = Q_\varepsilon(r)\,[\mathbf{E}] \tag{5}$$

where the $Q_\varepsilon(r)$ matrix is a 3×3 block matrix such as:

$$Q_\varepsilon = \begin{pmatrix} Q_{\varepsilon,\mathrm{rr}} & Q_{\varepsilon,\mathrm{r}\theta} & 0 \\ Q_{\varepsilon,\theta\mathrm{r}} & Q_{\varepsilon,\theta\theta} & 0 \\ 0 & 0 & Q_{\varepsilon,\mathrm{zz}} \end{pmatrix} \tag{6}$$

with $Q_{\varepsilon,\mathrm{rr}} = [\![\varepsilon]\!][\![N_\theta^2]\!] + [\![\frac{1}{\varepsilon}]\!]^{-1}[\![N_r^2]\!]$, $Q_{\varepsilon,\theta\theta} = [\![\varepsilon]\!][\![N_\mathrm{r}^2]\!] + [\![\frac{1}{\varepsilon}]\!]^{-1}[\![N_\theta^2]\!]$, $Q_{\varepsilon,\mathrm{r}\theta} = Q_{\varepsilon,\theta\mathrm{r}} = -([\![\varepsilon]\!] - [\![\frac{1}{\varepsilon}]\!]^{-1})[\![N_\mathrm{r}N_\theta]\!]$ and $Q_{\varepsilon,\mathrm{zz}} = [\![\varepsilon]\!]$. Since the matrix Q_ε contains the Toeplitz matrices $[\![N_r^2]\!]$, $[\![N_\theta^2]\!]$ and $[\![N_r N_\theta]\!]$ deduced from the normal vector components defined only on the surface S, we have to extend their definition in the entire modulated area ($R_{\min} < r < R_{\max}$) by introducing a new vector continuous across the diffracting surface S and defined by: $\forall r \in [R_{\min}, R_{\max}]$, $\mathbf{N}(r,\theta) = \frac{\mathbf{grad}(f)}{|\mathbf{grad}(f)|}$. Moreover, we may notice that the classical differential method which only applies Laurent's rule gives $[\mathbf{D}] = [\![\varepsilon]\!][\mathbf{E}]$.

Differentiating the Fourier developments given by equation (1) with respect to t, θ and z, Maxwell equations written in cylindrical coordinates are combined with Equation (5) in order to obtain the following set of first-order differential equations:

$$\frac{\mathrm{d}[F(r)]}{\mathrm{d}r} = \mathrm{i}\mathcal{M}(r)\,[F] \tag{7}$$

with the vector $[F]$ defined by

$$[F] = \begin{pmatrix} [E_\theta] \\ [E_z] \\ [H_\theta] \\ [H_z] \end{pmatrix} \tag{8}$$

and

$$\mathcal{M}(\mathrm{r})=\begin{pmatrix} -\frac{1}{r}\alpha {Q_{\varepsilon,rr}}^{-1} Q_{\varepsilon,r\theta}+\frac{i}{r} I_d & 0 & \frac{\beta}{\omega r}\alpha {Q_{\varepsilon,rr}}^{-1} & \omega\mu_0 I_d-\frac{\alpha}{\omega r^2} {Q_{\varepsilon,rr}}^{-1}\alpha \\ -\beta {Q_{\varepsilon,rr}}^{-1} Q_{\varepsilon,r\theta} & 0 & \frac{\beta^2}{\omega} {Q_{\varepsilon,rr}}^{-1}-\omega\mu_0 I_d & -\frac{\beta}{r\omega} {Q_{\varepsilon,rr}}^{-1}\alpha \\ -\frac{\beta}{\mu_0\omega r}\alpha & \frac{\alpha^2}{\omega\mu_0 r^2}+\omega Q_{\varepsilon,zz} & \frac{i}{r} I_d & 0 \\ \omega\left(Q_{\varepsilon,\theta\theta}-Q_{\varepsilon,\theta r} {Q_{\varepsilon,rr}}^{-1} Q_{\varepsilon,r\theta}\right)-\frac{\beta^2}{\mu_0\omega} I_d & \frac{\beta}{\mu_0\omega r}\alpha & Q_{\varepsilon,\theta r} {Q_{\varepsilon,rr}}^{-1}\beta & -Q_{\varepsilon,\theta r} {Q_{\varepsilon,rr}}^{-1}\frac{\alpha}{r} \end{pmatrix} \tag{9}$$

in which α is a diagonal matrix such that $(\alpha)_{nm}=n\delta_{nm}$ and I_d is the identity matrix. It's worth noticing that the $\mathcal{M}(r)$ matrix depends only on the r-coordinate and that its size is $4(2N+1)\times 4(2N+1)$. The radial components of the electric and magnetic fields can be deduced from the other components by

$$[E_r]={Q_{\varepsilon,rr}}^{-1}\left(\frac{\beta}{\omega}[H_\theta]-\frac{\alpha}{r\omega}[H_z]-Q_{\varepsilon,r\theta}[E_\theta]\right) \tag{10}$$

and

$$[H_r]=\frac{1}{\mu_0\omega}\left(\frac{\alpha}{r}[E_z]-\beta[E_\theta]\right) \tag{11}$$

2.3. RESOLUTION OF THE BOUNDARY-VALUE PROBLEM

The differential set given by the Equation (7) and Equations (10) and (11) describes the behaviour of the electromagnetic fields in the modulated area. Concerning the homogeneous and isotropic regions (int) and (ext), Maxwell equations reduce to a set of independent Bessel equations (second order differential equations) for the z-components of the electromagnetic fields (E_z and H_z). Their explicit solutions, from which we deduced the expressions of the other components of the electromagnetic fields, contain linear combinations of Bessel functions (J_n) and Hankel functions (H_n^+). Introducing the vector $[\mathrm{V}^{(j)}(r)]$ containing the components $A_{e,n}^{(j)}J_n\left(k_{tj}\mathrm{r}\right)$, $A_{h,n}^{(j)}J_n\left(k_{tj}r\right)$, $B_{e,n}^{(j)}H_n^+\left(k_{tj}r\right)$ and $B_{h,n}^{(j)}H_n^+\left(k_{tj}r\right)$ with $j=$ int or ext, we obtain in a matrix form

$$[F]=\Psi^{(j)}(r)\left[V^{(j)}\right] \tag{12}$$

with the matrix $\Psi^{(j)}(\mathrm{r})$ defined by

$$\Psi^{(j)}(r) = \begin{pmatrix} \frac{1}{r}p^{(j)} & q_e^{(j)} & \frac{1}{r}p^{(j)} & q_h^{(j)} \\ I_d & 0 & I_d & 0 \\ -\frac{\varepsilon_j}{\mu_0}q_e^{(j)} & \frac{1}{r}p^{(j)} & -\frac{\varepsilon_j}{\mu_0}q_h^{(j)} & \frac{1}{r}p^{(j)} \\ 0 & I_d & 0 & I_d \end{pmatrix} \tag{13}$$

in which $(p^{(j)})_{nm} = -\frac{\beta}{k_{tj}^2} n\delta_{nm}$, $\left(q_e^{(j)}\right)_{nm} = -\frac{i\omega\mu_0}{k_{tj}^2}\left[\frac{n}{r} - k_{tj}\frac{J_{n+1}(k_{tj}r)}{J_n(k_{tj}r)}\right]\delta_{nm}$, $\left(q_h^{(j)}\right)_{nm} = -\frac{i\omega\mu_0}{k_{tj}^2}\left[\frac{n}{r} - k_{tj}\frac{H_{n+1}^+(k_{tj}r)}{H_n^+(k_{tj}r)}\right]\delta_{nm}$, $k_{tj}^2 = k_j^2 - \beta^2$ and $k_j^2 = \omega^2\mu_0\varepsilon_j$. We observe that the size of vectors $[F]$ and $[V^{(j)}]$ is $4(2N+1)$. The amplitudes $A_{e,n}^{(j)}$, $A_{e,n}^{(j)}$, $A_{e,n}^{(j)}$ and $A_{e,n}^{(j)}$ for both homogeneous and isotropic regions ($j =$ int or ext) are the unknown quantities to be determined.

Unfortunately, the differential set described by the Equation (7) has no explicit solutions. We can't apply the boundary-value problem at the circular circle $C_{\min}$ and $C_{\max}$. To this aim, the differential set is resolved with a shooting method which changes the present boundary-value problem into an initial-value problem. At the end of the integration from $r = R_{\min}$ to $r = R_{\max}$ starting with the $\Psi^{(j)}(r)$ matrix as a set of initial independent vectors, the numerical results give the transmission matrix or T-matrix of the device which links the field at $R_{\min}$ with the field at $R_{\max}$. However, numerical contaminations can occur during the integration process which makes the T-matrix ill-conditioned. In order to avoid such problems, we use the S-propagation algorithm (Li 1996b) which involves splitting the modulated area into several slices and in normalizing the T-matrix of each layer using a well-conditioned S-matrix. The S-matrix links the diffracted fields in the interior and the exterior regions with the source waves:

$$\begin{pmatrix} \vdots \\ B_{e,n}^{(\text{ext})} H_n^+\left(k_{t,\text{ext}} R_{\max}\right) \\ \vdots \\ B_{h,n}^{(\text{ext})} H_n^+\left(k_{t,\text{ext}} R_{\max}\right) \\ \vdots \\ A_{e,n}^{(\text{int})} J_n\left(k_{t,\text{int}} R_{\min}\right) \\ \vdots \\ A_{h,n}^{(\text{int})} J_n\left(k_{t,\text{int}} R_{\min}\right) \\ \vdots \end{pmatrix} = \mathbf{S} \begin{pmatrix} \vdots \\ B_{e,n}^{(\text{int})} H_n^+\left(k_{t,\text{int}} R_{\min}\right) \\ \vdots \\ B_{h,n}^{(\text{int})} H_n^+\left(k_{t,\text{int}} R_{\min}\right) \\ \vdots \\ A_{e,n}^{(\text{ext})} J_n\left(k_{t,\text{ext}} R_{\max}\right) \\ \vdots \\ A_{h,n}^{(\text{ext})} J_n\left(k_{t,\text{ext}} R_{\max}\right) \\ \vdots \end{pmatrix} \tag{14}$$

Knowing that the modes describe the field without sources, we search the amplitudes $A_{e,n}^{(\text{int})}$, $A_{h,n}^{(\text{int})}$ and $B_{e,n}^{(\text{ext})}$, $B_{h,n}^{(\text{ext})} \forall$n being solutions of the following homogeneous set of equations deriving from Equation (14):

$$S^{-1}\begin{pmatrix} \vdots \\ B_{e,n}^{(\mathrm{ext})} H_n^+\left(k_{t,\mathrm{ext}} R_{\max}\right) \\ \vdots \\ B_{h,n}^{(\mathrm{ext})} H_n^+\left(k_{t,\mathrm{ext}} R_{\max}\right) \\ \vdots \\ A_{e,n}^{(\mathrm{int})} J_n\left(k_{t,\mathrm{int}} R_{\min}\right) \\ \vdots \\ A_{h,n}^{(\mathrm{int})} J_n\left(k_{t,\mathrm{int}} R_{\min}\right) \\ \vdots \end{pmatrix} = \begin{pmatrix} \vdots \\ 0 \\ \vdots \\ 0 \\ \vdots \\ 0 \\ \vdots \\ 0 \\ \vdots \end{pmatrix} \tag{15}$$

Consequently, we search the effective index which nullifies the determinant of the inverse of the S-matrix. We can notice that the modal fields correspond to the eigenvectors with the null eigenvalues of the S-matrix existing at these values of the effective index.

2.4. DEVICES WITH SUB-PERIODICITY ACCORDING TO θ

Most of MOFs studied by well-established numerical methods have shapes periodic with respect to θ. In the Fourier space, this property implies the widening of the function spectrum. In fact, if we consider the Fourier components $\tilde{f}'_n$ of a function $\tilde{f}$ calculated on a sub-period T of 2π (such that $N_{\mathrm{T}}T = 2\pi$ where N_T is the number of sub-periodicity), then the Fourier components $\tilde{f}_n$ of the same function but calculated on the 2π period are deduced from $\tilde{f}'_n$ by the following relation if $n = kN_T (\forall k \in \mathbb{N})$ then $\tilde{f}_n = \tilde{f}'_k$ and $\tilde{f}_n = 0$ else. Consequently, the Toeplitz matrix of the function $\tilde{f}$ is made of non-null diagonals regularly separated by $N_T - 1$ null diagonals and becomes block-diagonalizable. Since this matrix structure is preserved when such a matrix is inverted or when two such matrices are multiplied as occurs in the $Q_\varepsilon(r)$ matrix and then in the $\mathcal{M}(r)$ matrix, the differential set given by (7) is split into N_T independent differential sub-sets. Generally, the integration computation time depends on the cube of the matrix integration size. Consequently, the time of a successive integration of each differential sub-set is N_T^2 times faster than the global integration one.

3. Numerical applications

3.1. VALIDATION STUDIES

In order to validate our numerical code using the FFF method, we compare its results with a well-established method, the Multipole Method

(Kuhlmey *et al.* 2002; White *et al.* 2002; Zolla *et al.* 2005). The MM requires MOF inclusions to be included using non-overlapping circular cylinders, that is why we first chose to study a MOF composed of six identical circular cylinders with a diameter $d = 1\,\mu$m located at the same distance from the origin (pitch) $\Lambda = 2.3\,\mu$m (see Fig. 3). Concerning the sub-periodicity of the device for the FFF method, we note that the number of sub-periodicity is $N_T = 6$, i.e. the device contains one circular inclusion in the sub-period $T = \pi/3$. Moreover, this fiber follows the C_{6v} symmetries. In addition, we know that the fundamental mode is doubly degenerate. Its field component E_z belong to the $C3/4$ symmetry classes: one has the C4 symmetry (symmetric according to the Y-axis: $u(\pi - \theta) = u(\theta)$ and anti-symmetric according to the X-axis: $u(-\theta) = -u(\theta)$) and the other one has the C3 symmetry (anti-symmetric according to the Y-axis and symmetric according to the X-axis) (Kuhlmey *et al.* 2002; White *et al.* 2002; Zolla *et al.* 2005).

We are first interested in the fundamental mode for which the MM gives an effective index equal to $n_{\text{eff}} = 1.42078454 + i\,7.20952 \times 10^{-4}$ for $\lambda_0 = 1.56\,\mu$m. The FFF method algorithm finds the minima (associated with the fundamental mode) in the map of the determinant of the S^{-1}-matrix and then uses a complex regression algorithm to better locate this effective index. For $N = 60$, the searching algorithm in the FFF method numerical code computes the determinant map illustrated in Fig. 4 and finds the value $n_{\text{eff}} = 1.42078315 + 7.20465 \times 10^{-4}$. The relative discrepancy of the FFF method $|n_{\text{eff}}|$ value compared with the MM is of the order 10^{-4}. The corresponding normalized $|E_z|$ maps for the two degenerate fields calculated from the eigenvectors of the S^{-1} matrix evaluated at this n_{eff} value are shown in Figs. 5 and 6.

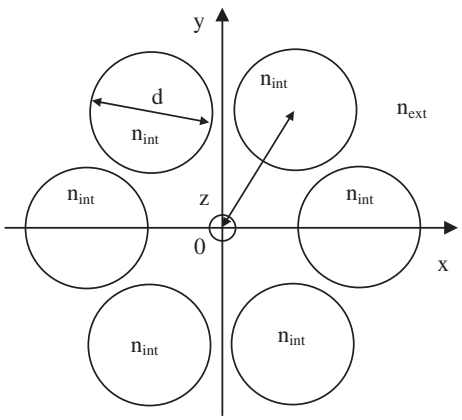

Fig. 3. Cross section of six circular cylinders with $d = 1\,\mu$m, $\Lambda = 2.3\,\mu$m, $n_{\text{int}} = 1$ and $n_{\text{ext}} = 1.4439$, and notations.

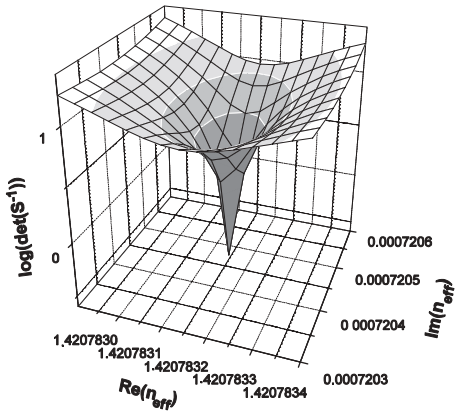

Fig. 4. Determinant map according to the effective index of the fundamental mode.

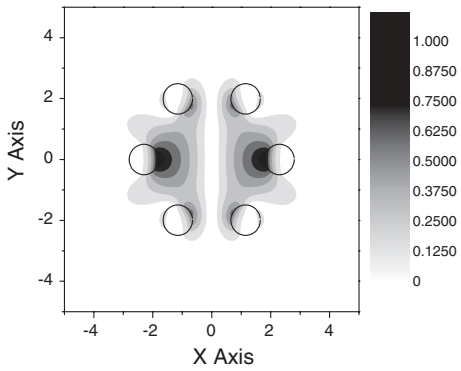

Fig. 5. Normalized $|E_z|$ field map for the degenerate fundamental mode, symmetry class C3.

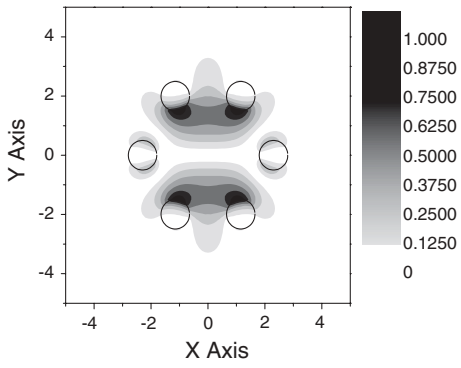

Fig. 6. Normalized $|E_z|$ field map for the degenerate fundamental mode, symmetry class C4.

In order to evaluate the accuracy and the interest of the FFF method, we test the convergence with respect to the development order N. Fig. 7 shows that the effective index calculated by the FFF method converges to the MM value faster than when using the classical differential method (Vincent *et al.* 1972). The relative discrepancy of the $|n_{\text{eff}}|$ value for the FFF method compared with the MM reaches the value of 5.10^{-6} for $N = 90$.

In addition, the FFF method may be used with other geometrical symmetries. For instance, we consider a MOF with a C_{2v} symmetry. The device remains the same as shown previously ($\lambda_0 = 1.56\,\mu$m) but the diameters of both circles on the x-axis ($1.4\,\mu$m) is larger than the other ones ($1\,\mu$m). In this case, the number of sub-periodicity N_{T} becomes equal to 2 and the sub-period T is equal to $\pi/2$. The C3 and C4 symmetry class fields become non-degenerate modes. For the C3 symmetry class with $N = 60$, the FFF method finds the value $n_{\text{eff}} = 1.41792219 + 5.11104.10^{-4}$ while the MM value is $n_{\text{eff}} = 1.4179230 + 5.114651.10^{-4}$. For the C4 symmetry class, the FFF method numerical program finds $n_{\text{eff}} = 1.41845587 + 5.27516.10^{-4}$ while the MM value is $n_{\text{eff}} = 1.4184564 + 5.2785301.10^{-4}$. Figs. 8 and 9 illustrate the normalized $|E_z|$ maps respectively for the C3 and C4 symmetry classes.

3.2. A MOF WITH SIX SECTORIAL CYLINDERS

The FFF method is well-adapted for arbitrary cross section device. One of the simpliest inclusion that this method can consider consists of a sectorial inclusion because the Toeplitz matrices $[\![N_r^2]\!]$, $[\![N_\theta^2]\!]$ and $[\![N_r N_\theta]\!]$ are easy

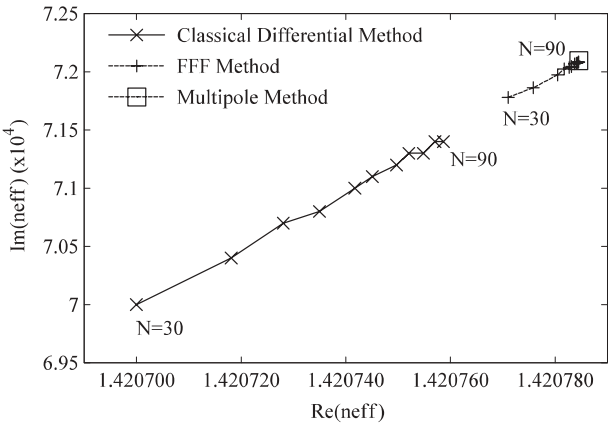

Fig. 7. Convergence test of the effective index according to N for the FFF method and the Classical method compared with the Multipole Method value.

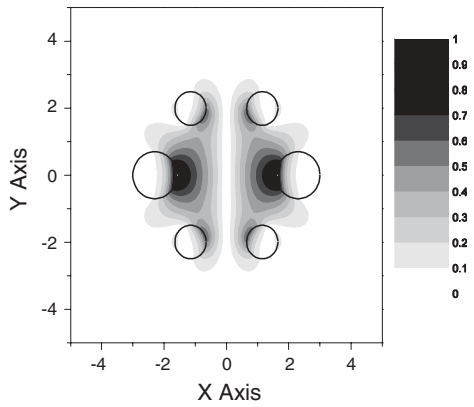

Fig. 8. Normalized $|E_z|$ field map for the mode belonging to the symmetry class C3.

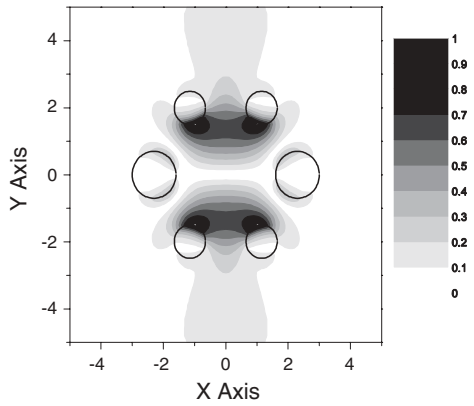

Fig. 9. Normalized $|E_z|$ field map for the mode belonging to the symmetry class C4.

to determine in this case. For a first computation, we are interested in a six sectorial cylinder MOF defined in the same way than the previous six circular cylinder MOF : the cross section filling ratio is identical for both sectorial and circular cylinders ($R_0 = 1.8\,\mu$m, $L = 1\,\mu$m and $\theta_m = 9.7826^\circ$, see figure 10 for notations). For $N = 60$, the effective index of the degenerate fundamental mode is $n_{\text{eff}} = 1.4205064 + 7.63909.10^{-4}$. The corresponding normalized $|E_z|$ field map belonging to the C3 symmetry class is illustrated in the Fig. 11.

4. CONCLUSION

We conclude that the Fast Fourier Factorization method provides faster convergence than the classical differential method for numerical solutions

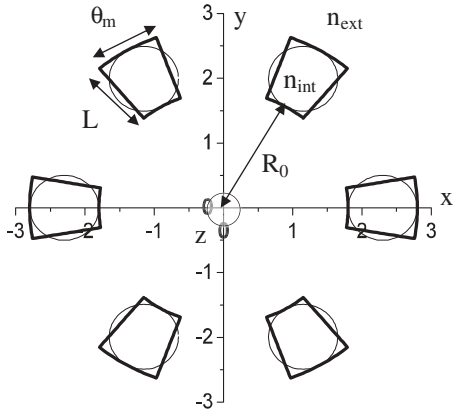

Fig. 10. Cross section of six circular cylinders with $R_0 = 1.8\,\mu$m, $L = 1\,\mu$m, $\theta_m = 9.7826^\circ$, $n_{\text{int}} = 1$ and $n_{\text{ext}} = 1.4439$, and notations.

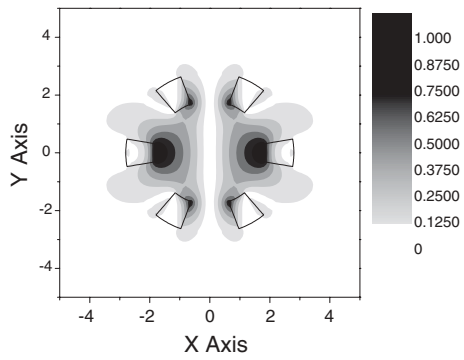

Fig. 11. Normalized $|E_z|$ field map for the degenerate fundamental mode, symmetry class C3 for a C_{6v} sectorial MOF.

of Maxwell's equations in a truncated space. For reasonable values of the Fourier development truncation order, the FFF method produces highly accurate predictions of the effective indices. In addition, the FFF method is not limited to profiles of circular-cylinder MOFs that have already been well studied with the Multipole Method. In future works, we plan to establish the dispersion properties of these new structures.

References

Boyer, P., E. Popov, M. Nevière and G. Tayeb. *J. Opt. Soc. Am. A*. **21** 2146, 2004.

Kuhlmey, B.T., T.P. White, G. Renversez, D. Maystre, L.C. Botten, C.M. de Sterke and R.C. McPhedran. *J. Opt. Soc. Am. B*. **19** 2331, 2002.

Li, L. *J. Opt. Soc. Am. A*. **13** 1870, 1996a.

Li, L. *J. Opt. Soc. Am. A*. **13** 1024, 1996b.
Nevière, M. E. Popov. *Light Propagation in Periodic Media: Differential Theory and Design*, Marcel Dekker, Inc. New-York, 2003.
Vincent, P. and R. Petit. *Opt. Commun*. **5** 261, 1972.
White, T.P., B.T. Kuhlmey, R.C. McPhedran, D. Maystre, G. Renversez, C.M. de Sterke and L.C. Botten. *J. Opt. Soc. Am. B*. **19** 2322, 2002.
Zolla, F., G. Renversez, A. Nicolet, B. Kuhlmey, S. Guenneau and D. Felbacq. *Foundations of Photonic Crystal Fibers*, Imperial College Press, 2005.